Ca^{2+}-Doped $CeBr_3$ Scintillating Material

Paul Guss,* Sanjoy Mukhopadhyay,† Ding Yuan†† Patrick Doty†††

** Nevada National Security Site, Remote Sensing Laboratory–Nellis, P.O. Box 98521, M/S RSL-09, Las Vegas, NV 89193-8521, USA, gusspp@nv.doe.gov*
† Nevada National Security Site, Remote Sensing Laboratory Andrews Operation, Building 1783, Arnold Ave, Joint Base Andrews, MD 20762, mukhops@nv.doe.gov
†† Nevada National Security Site, P.O. Box 98521, M/S NLV076 Las Vegas, NV 89193-8521, USA, yuand@nv.doe.gov
†††Sandia National Laboratories, California, Materials Chemistry Department, P.O. Box 969, Livermore, CA 94551-0969, USA, fpdoty@sandia.gov

INTRODUCTION

This paper presents on the scintillation properties of $CeBr_3$ crystals grown with the divalent dopant Ca^{2+}. For this study, Dynasil Radiation Monitoring Devices, Inc. (RMD) grew small diameter (up to ~1 cm) single crystals of $CeBr_3$ doped with Ca^{2+}. The aliovalently calcium-doped cerium tribromide ($CeBr_3$:Ca^{2+}) crystals were prepared according to careful theoretical modeling and delivered to the Remote Sensing Laboratory (RSL) for assessment and evaluation (Fig. 1). $CeBr_3$:Ca^{2+} has a hexagonal crystal structure identical to uranium trichloride (UCl_3). The reliability of large crystals may be questionable and their manufacturing yield may be low, as hexagonal crystals may fracture easily [1,2]. However, increasing the fracture toughness of the crystals may lead to significant gains in the practical scale for $CeBr_3$ scintillators [3]. Aliovalent substitution, in which an ion of different valence (e.g., Ca^{2+} for Ce^{3+} in $CeBr_3$) replaces a host ion is a more potent method of strengthening than isovalent substitution (i.e., replacing a fraction of ions with like-valence ions). In this approach, the formation of intrinsic defects necessary to maintain charge neutrality results in complexes with long-range interactions in the crystal. The elastic interaction with dislocations may result an increase in hardening rate [4].

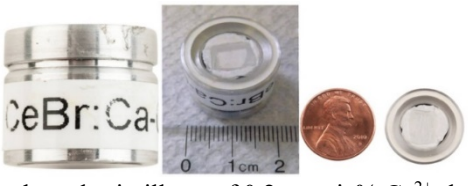

Fig. 1. Packaged scintillator of 0.2 atomic% Ca^{2+}-doped $CeBr_3$.

Because $CeBr_3$ already exhibits superior scintillation characteristics [5,6], the alloying element(s) used to strengthen the crystal must not degrade the scintillation properties. Aliovalent alloying provides more strengthening than isovalent alloying. The solid solution strengthening τ based on lattice distortions due to some small concentration of dopant approximately is

$$\tau = \gamma \bullet Gc^{½}, \quad (1)$$

where G is the shear modulus, c is the concentration of solute in atomic fraction, and γ is a proportionality constant [7,8]. For spherically symmetric distortions, such as those found in isovalent alloying, γ typically takes on values that are significantly smaller than unity, from 10^{-4} to 10^{-6}. For tetragonal lattice distortions, such as those created from solute atoms of a different valence, γ can be nearly unity. Therefore, aliovalent alloying is more effective for a given concentration of solute [8].

EXPERIMENT

RMD grew and packaged the calcium-doped $CeBr_3$:Ca^{2+} crystallite. Sandia National Laboratories (SNL) performed density functional theory (DFT) model calculations for a nominal doping (i.e., 2%) of calcium in $CeBr_3$. This helped assess what doping concentration would lead to changes in optical and mechanical properties. RMD assessed crystal growth strategies for performing growth with lower concentrations of calcium. SNL measured the calcium concentration by the inductively coupled plasma mass spectrometry.

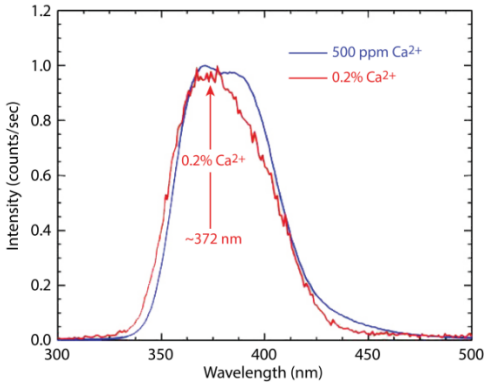

Fig. 2. Emission spectrum measured with 6 × 2 mm 0.2 atomic% Ca^{2+}-doped $CeBr_3$ crystal in the permanent canister compared to a similar measurement for a 500 ppm Ca^{2+}-doped $CeBr_3$ crystal.

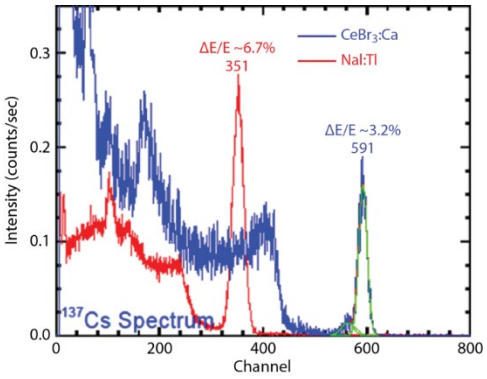

Fig. 3. Light output measurement relative to NaI:Tl indicates 62,000 photons per MeV for Ca^{2+}-doped $CeBr_3$ crystal.

RSL assessed the RMD crystal. RSL acquired spectra with different isotopes using the RMD crystal using the techniques described by Guss [3,9]. Fig. 2 presents the emission spectrum for this crystallite. These results are consistent with recent findings [10]. The increase in doping level led to a slight blue shift in the emission spectrum. Fig. 3 shows a light output measurement for the crystallite estimated at 62,000 photons per MeV based on comparison to the thallium-doped sodium iodide (NaI:Tl) light yield.

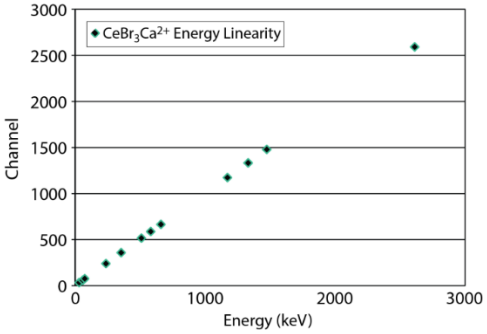

Fig. 4. Relative light yield proportionality of 0.2 atomic% Ca^{2+}-doped $CeBr_3$.

Proportionality of light yield is one area of performance where Ce-doped and Ce-based lanthanide halides excel. Maintaining proportionality is key to producing a strong, high-performance scintillator. Measurements for relative light yield proportionality for both doped and undoped samples of $CeBr_3$ ensured no loss in performance resulted by aliovalently doping the crystal. The light output and proportionality, however, appear to be like $CeBr_3$. There was a reduced yield at low energy. Relative light yields proportionality measurements suggest that dopants do not significantly affect proportionality at higher energies. **Fig. 4** presents a plot of light yield proportionality for a doped sample.

RSL completed additional testing and evaluation of the new crystal as well as the assessment of benchmarking spectroscopy data. Fig. 4 summarizes the results, which present energy resolution as a function of energy. Fig. 5 shows a typical spectroscopy result using a ^{137}Cs radiation source for our crystallites. We obtain 4.5% for the packaged crystallite. Spectra obtained for ^{241}Am, ^{60}Co, ^{228}Th, and background further exemplified $CeBr_3$:Ca^{2+} performance over a broader energy range. The radiation source spectra measurements represented a data acquisition for 3600 seconds with the radiation source in contact with the crystal face using typical source strengths of several μCi. The laboratory background acquisition time was 3×10^5 sec. Obviously, the packaging of the crystallite impacted the performance of $CeBr_3$:Ca^{2+}.

We have observed Ca^{2+} to be a most promising dopant, since it significantly reduces the nonproportionality and improves the energy resolution of pure $CeBr_3$. We have measured the nonproportionality in the energy range from 32 keV up to 1274 keV. At 32 keV, the $CeBr_3$:Ca^{2+} deviates about 4% from the ideal case (10% for pure $CeBr_3$). We achieved an excellent energy resolution of 3.2% at 662 keV and light output of ~ 62,000 photons/MeV [11,12].

We sought to achieve ultralow activity and high strength cerium bromide scintillators through a program of refining and alloying with aliovalent strengthening agents (substituents with a different valence than the host lattice). $CeBr_3$ is a self-activated lanthanide scintillator, which has received considerable recent attention [13] due to proportionality and energy resolution for gamma spectroscopy far superior to NaI:Tl. Because the material possesses no intrinsic radioactivity, $CeBr_3$ has a high potential to outperform scintillators such as cerium-activated lanthanum tribromide or lanthanum-based elpasolites [14], making it an excellent candidate for gamma spectrometers for passive detection and identification of special nuclear material [15,16]. However, due to its hexagonal crystal structure (UCl_3), pure $CeBr_3$ can fracture during crystal growth, detector fabrication, and subsequent use under field conditions, thus impacting manufacturing yield and reliability for large crystals [2].

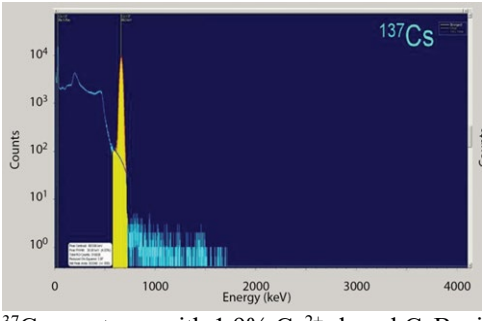

Fig. 5. ^{137}Cs spectrum with 1.9% Ca^{2+}-doped $CeBr_3$ in the permanent canister.

Aliovalent substitution, in which an ion of different valence (e.g., Cd^{2+} for Ce^{3+} in $CeBr_3$) replaces a host ion, is a more potent method of strengthening than isovalent substitution (i.e., replacing a fraction of ions with like-

valence ions). The formation of intrinsic defects necessary to maintain charge neutrality results in complexes with long-range interactions in the crystal. The elastic interaction (tetragonal distortion) with dislocations may result in an increase in hardening rate [4]. Concentration levels necessary to increase the yield strength by an order of magnitude may be in the 100–500 ppm range (0.01%–0.05%) for aliovalent substitution, whereas isovalent substitution may require 10%–50% to achieve the same effect.

For these reasons, aliovalent substitution may improve the strength of $CeBr_3$. SNL demonstrated success with this approach, achieving a dramatic reduction of fracture in aliovalent alloys compared with pure $CeBr_3$ crystals [8]. Prototype high-purity $CeBr_3$ ingots compounded with the addition of 2% of $CaBr_2$ added provided the charge in a closed ampoule before melting and solidification in a gradient-freeze process. Pure $CeBr_3$ ingots solidified under these conditions were severely fractured, yielding only centimeter-sized shards. The lesson learned was that 2% was too high of a charge for the calcium. We performed mass analysis of the material and recalculated the DFT with a lower charge of calcium. We performed an assessment of the spectroscopic performance of $CeBr_3$:Ca shards.

RMD grew, packaged, and delivered to RSL the 2% calcium-doped $CeBr_3$:Ca crystallite. Several minor tasks remained to complete characterization of the calcium-doped crystal. SNL performed DFT model calculations with less dilute doping of calcium in $CeBr_3$. This helped assess what doping concentration would lead to changes in optical and mechanical properties. RSL assessed the spectroscopic performance of the crystal. RSL acquired spectra with different isotopes using the RMD crystal using the techniques described by Guss [3,17,18]. Fig. 2 shows the emission spectrum for this crystallite. Fig. 3 shows a light output measurement for the crystallite estimated at 62,000 photons per MeV based on light yield.

Figs. 3 presents the ^{137}Cs radiation source spectrum. A slight degradation in performance is associated with the permanent package of the crystal.

CALCIUM CONCENTRATION

We have measured the calcium concentration in the $CeBr_3$ by the inductively coupled plasma mass spectrometry (ICP-MS) technique from the crystals prepared by RMD. ICP-MS is a type of mass spectrometry capable of detecting metals and several non-metals at concentrations as low as one part in 10^{12} (part per trillion). SNL performed the ICP-MS. SNL also calculated a DFT model with less dilute doping (i.e., something less than 2%) of calcium in $CeBr_3$. SNL analyzed the concentration of calcium in the crystals. We used the average calcium weight % concentration, x = 0.000214, in our complex of $Ce_{(1-x)}Ca_xBr_{(3-x)}$, to evaluate the formula for atomic percentage:

$$\text{Atomic \%} = 40.078x/[140.116\,(1-x) + 40.078x + 79.904\,(3-x)] = 0.00228 = 0.228\% \quad (2)$$

Based on our measurements, using three different samples (~0.2 grams), we have three consistent data sets indicating that the calcium concentration in these crystals is 0.0214 ±0.0102 wt.% (one σ) by weight, which corresponds to an atom percentage of 0.228 at.%.

Results plotted in Fig. 6 indicate the approximate solidus, liquidus, and eutectic lines. Not plotted are some additional data taken at 20% and 30%, which indicate the liquidus continues the near-linear trend. Note that our current experimental upper bound for the solid solubility is the data point at 2.35%, which must lie well within the α + β field, with the detection of the eutectic temperature T_e. This concentration is considerably less than the intersection of the extrapolated solidus and the eutectic temperature; therefore, the solidus line is clearly nonlinear and probably exhibits retrograde solubility well below the melting point of pure $CeBr_3$, as observed for sparingly soluble impurities in other systems. This behavior characterizes a variation of the segregation coefficient with temperature, as analyzed by Hall [19]. For example, the maximum solid solubility for sparingly soluble impurities in silicon and germanium follow a simple empirical correlation with k_0, the limiting equilibrium segregation coefficient, as C_L approaches 0: $C_{S,max} = k_0/10$ [20]. Based on this relation, the solidus extrapolates to $k_{eff}/10 = 1.1\%$ at the eutectic temperature to estimate the minimum extent of the eutectic line towards the $CeBr_3$ side of the phase diagram (Fig. 6).

The eutectic composition extrapolated from the points plotted is near 37% calcium; however, the nominal 20% and 30% data indicate it could be near 50%. Future experimentation will better accurately determine both the eutectic composition and the β phase, which in fact could turn out to be a ternary such as $CaCeBr_5$ or Ca_2CeBr_7.

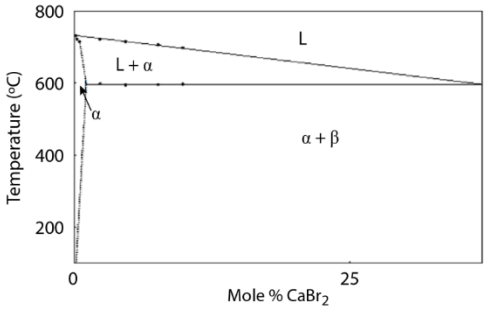

Fig. 6. Phase diagram for $CeBr_3$-$CaBr_2$.

RESULTS

SNL performed microhardness measurements to see if the aliovalent approach hardened the crystal as expected. SNL measured the microhardness (Vickers hardness [21]) and indentation toughness of these samples. Due to the size limitation, we could not obtain enough statistics and

confidence on these measured values. Therefore, we do not report the results here. Future work should include studies in correlation between sheer strength and Ca^{2+} concentration.

Based on the recent literature on strengthening mechanisms [22], there are compelling requirements to research and several ideas, questions, and answers to share. Sinha's paper on aliovalent strengthening of CaF_2 attempts to determine mechanisms for low and high temperatures. Sinha and Nicholson [22] found that Y(III) gave an order of magnitude greater increase in critical resolve shear stress than Na(I). They conclude the long-range retarding force on dislocations at high temperature is likely due to the induced reorientation of Na(I)/F-vacancy or Y(III)/F-interstitial dipoles in the stress fields of moving dislocations (Snoek effect). This suggested role of the Snoek effect [23] is in accord with analysis of the athermal regime in recent papers on Y stabilized zirconia and other materials [5,13,24–27].

SUMMARY

To summarize, new DFT simulations demonstrate a capability for predicting properties of doped $CeBr_3$ materials that is unavailable elsewhere but is critical to study the property-limiting valence phenomena in ionic compounds. During this project, we assessed concentrations and the solubility limit. RSL benchmarked the Ca^{2+}-doped $CeBr_3$ crystal. The Ca^{2+}-doped $CeBr_3$ crystal has improved energy resolution (i.e., 3.2%) and linearity over the pure $CeBr_3$ crystal.

ACKNOWLEDGMENT

Marlene Bencomo (University of New Mexico, Albuquerque) assisted with IC-PMS analysis. This work was done by Mission Support and Test Services, LLC, under Contract No. DE-NA0003624 with the U.S. Department of Energy and supported by the Site-Directed Research and Development Program. DOE/NV/03624--0997. The United States Government retains and the publisher, by accepting the article for publication, acknowledges that the United States Government retains a non-exclusive, paid-up, irrevocable, world-wide license to publish or reproduce the published form of this manuscript, or allow others to do so, for United States Government purposes.

REFERENCES

1. F. DOTY, et al., *Proc. SPIE* **6707** (2007) 670705:1–11.
2. F. DOTY, et al., *Proc. Mat. Res. Soc.* **1038** (2008) 1–8.
3. P. GUSS, et al., *Site-Directed Research and Development*, FY 2012, National Security Technologies, LLC, Las Vegas, Nevada, 2013, 11–19.
4. B. J. PLETKA, et al., *Physica Status Solidi* **39**, 1 (1977) 301–311.
5. K. S. SHAH, et al., *IEEE Trans. Nucl. Sci*. **52**, 6 (2005) 3157–3159.
6. S. RA, et al., *IEEE Trans. Nucl. Sci.* **55**, 3 (June 2008) 1221–1224.
7. T. H. COURTNEY, *Mechanical Behavior of Materials*, 2nd edition, Waveland, Long Grove, Illinois, 2000, 232.
8. M. J. HARRISON, et al., *Proc. SPIE* **7806** (2010) 78060M–78060M-14.
9. P. P. GUSS, et al., *Nevada National Security Site–Directed Research and Development*, FY 2010, National Security Technologies, LLC, Las Vegas, Nevada, 2011, 55–64.
10. F. G. A. QUARATI, et al., *Nucl. Instrum. Methods Phys. Res. A* (2013) http://dx.doi.org/10.1016/j. nima.2013.08.005.
11. P. GUSS, et al., *Site-Directed Research and Development*, FY 2013, National Security Technologies, LLC, Las Vegas, Nevada (2014) 221–234.
12. U. SHIRWADKAR, et al., *Proceedings of the 20th Conference on Room-Temperature Semiconductor X- and Gamma-Ray Detectors*, IEEE, Seoul, South Korea (2013) N-4.
13. K. S. SHAH, et al., *IEEE Trans. Nucl. Sci.* **52**, 6 (2005) 3157–3159.
14. P. P. GUSS, et al., *Nucl. Instrum. Methods Phys. Res. A* **608**, 2 (2009) 297–304.
15. K. S. Shah, et al., *IEEE Trans. Nucl. Sci.* **51**, 5 (2004) 2395–2399.
16. P. P. GUSS, et al., *Proc. SPIE* **7805** (2010) L-1.
17. P. P. GUSS, et al., *Nevada National Security Site–Directed Research and Development,* FY 2010, National Security Technologies, LLC, Las Vegas, Nevada (2011) 55–64.
18. P. P. GUSS, *J. Appl. Phys.* **115**, 3 (2014) 034908-1.
19. R. N. HALL, *J. Phys. Chem. Solids* **3**, 1–2 (1957) 63–73.
20. S. FISCHLER, *J. Appl. Phys.* **33**, 4 (1962) 1615.
21. R. L. SMITH and G. E. SANDLAND, *Proceedings of the Institution of Mechanical Engineers*, **I** (1922) 623–641.
22. M. N. SINHA and P. S. NICHOLSON, *J. Mat. Sci.* **12**, 7 (1977) 1451–1462.
23. J. SNOEK, *Physica* **8**, 7 (1941) 711–733.
24. D. BAITHER, et al., *Mat. Sci. Eng.* **A233** (1997) 75–87.
25. D. H. LASSILA, et al., *Metallurgical and Materials Transactions* **33A** 11 (November 2002) 3457–3464.
26. C. MERCER, et al., *Proc. R. Soc. A* **463** (8 May 2007) 1393–1408, http://www.materials.ucsb.edu/MURI/papers/MerceretaI_PRS07.pdf, accessed December 12, 2013.
27. S. ARMENGOL, Latin American Congress on Biomedical Engineering 2007, Bioengineering Solutions for Latin America Health, *IFMBE Proceedings* **18** (2008) 671–675.